Cite as: S. Zhu *et al.*, *Science* 10.1126/science.aax0274 (2019).

Nearly quantized conductance plateau of vortex zero mode in an iron-based superconductor

Shiyu Zhu[1,2]*, Lingyuan Kong[1,2]*, Lu Cao[1,2]*, Hui Chen[1,2]*, Michał Papaj[5], Shixuan Du[1,2,3,6], Yuqing Xing[1,2], Wenyao Liu[1,2], Dongfei Wang[1,2], Chengmin Shen[1,3], Fazhi Yang[1,2], John Schneeloch[4], Ruidan Zhong[4], Genda Gu[4], Liang Fu[5], Yu-Yang Zhang[2,1,3]†, Hong Ding[1,2,3,6]†, Hong-Jun Gao[1,2,3,6]†

[1]Beijing National Laboratory for Condensed Matter Physics and Institute of Physics, Chinese Academy of Sciences, Beijing 100190, China. [2]School of Physical Sciences, University of Chinese Academy of Sciences, Beijing 100190, China. [3]CAS Center for Excellence in Topological Quantum Computation, University of Chinese Academy of Sciences, Beijing 100190, China. [4]Condensed Matter Physics and Materials Science Department, Brookhaven National Laboratory, Upton, NY 11973, USA. [5]Department of Physics, Massachusetts Institute of Technology, Cambridge, MA 02139, USA. [6]Songshan Lake Materials Laboratory, Dongguan, Guangdong 523808, China.

***These authors contributed equally to this work.**

†Corresponding author. Email: hjgao@iphy.ac.cn (H.-J.G.); dingh@iphy.ac.cn (H.D.); zhangyuyang@ucas.ac.cn (Y.-Y.Z.)

Majorana zero modes (MZMs) are spatially-localized zero-energy fractional quasiparticles with non-Abelian braiding statistics that hold promise for topological quantum computing. Owing to the particle-antiparticle equivalence, MZMs exhibit quantized conductance at low temperature. By utilizing variable-tunnel-coupled scanning tunneling spectroscopy, we study tunneling conductance of vortex bound states on $FeTe_{0.55}Se_{0.45}$ superconductors. We report observations of conductance plateaus as a function of tunnel coupling for zero-energy vortex bound states with values close to or even reaching the $2e^2/h$ quantum conductance (here e is the electron charge and h is Planck's constant). In contrast, no plateaus were observed on either finite energy vortex bound states or in the continuum of electronic states outside the superconducting gap. This behavior of the zero-mode conductance supports the existence of MZMs in $FeTe_{0.55}Se_{0.45}$.

Majorana zero modes (MZMs) obey non-Abelian statistics and have potential applications in topological quantum computation (*1*, *2*). In the past two decades, MZMs have been predicted in p-wave superconductors (*3*, *4*) and spin-orbit-coupled materials proximitized by s-wave superconductors (*5*–*8*). Experimental evidence for MZMs has been observed in various systems, including semiconductor-superconductor nanowires (*9*, *10*), topological insulator-superconductor heterostructures (*11*), and atomic chains on superconducting substrate (*12*, *13*). Recently, fully gapped bulk iron-based superconductors have emerged as a single-material platform for MZMs (*14*, *15*). Evidence for MZMs in topological vortices on the surface of $FeTe_{0.55}Se_{0.45}$ has been found by scanning tunneling microscopy/spectroscopy (STM/S) (*16*–*18*).

At sufficiently low temperatures, the conductance of an MZM exhibits a quantized plateau at the value of $2e^2/h$, where e is the electron charge and h is Planck's constant (*19*, *20*). This quantized Majorana conductance results from perfect resonant Andreev reflection guaranteed by the inherent particle-hole symmetric nature of MZM (*2*). A quantized conductance plateau has been observed in an InSb-Al nanowire system, consistent with the existence of MZMs (*21*). However, some alternative explanations have not been ruled out, *e.g.* the partially separated Andreev bound state (ps-ABS) can also lead to a quantized conductance plateau which is topological trivial (*22*–*24*). Iron-based superconductors, where STM/S experiments observed zero-bias conductance peaks (ZBCPs) (*16*–*18*, *25*), have large topological gaps (estimated at ~0.7 meV for Fe(Te,Se) in Ref. *16*) and offer the possibility of observing Majorana quantized conductance without contamination from low-lying Caroli-de Gennes-Matricon bound states (CBSs) (*16*, *18*). Results suggesting quantized conductance have been reported for $(Li_{0.84}Fe_{0.16})$OHFeSe (*26*).

Motivated by the above prospects, we employ a variable tunnel coupling STM/S method to study the Majorana conductance over a large range of tip-sample distance in vortex cores of $FeTe_{0.55}Se_{0.45}$ (Fig. 1A). The effective electron temperature (T_{eff}) of our STM is 377 mK as calibrated by tunneling into aluminum (fig. S1). In STM/S, the tunnel coupling can be continuously tuned by changing the tip-sample distance (d), which correlates with the tunnel-barrier conductance ($G_N \equiv I_t/V_s$, I_t is the tunneling current. V_s is the setpoint voltage) (*16*). With a 2 T magnetic field applied perpendicular to the sample surface, a sharp ZBCP is observed at a vortex core (Fig. 1B). This ZBCP neither disperses nor splits across the vortex core, as expected for an isolated MZM in a quantum-limited vortex (*16*–*18*, *25*). We perform tunnel-coupling dependent measurement on the observed ZBCP. By putting the STM tip at the center of a topological vortex (*18*), we record a set of dI/dV spectra with different tip-sample distances (Fig. 1C). The ZBCP remains a well-defined peak located at zero energy [voltage offset calibration under different tunnel couplings is

discussed in (*27*)]. More significantly, we observe a unique behavior of ZBCP under different G_N (Fig. 1C): the ZBCP peak height saturates at a relatively high tunnel coupling (Fig. 1F), whereas the high-bias conductance outside the superconducting gap increases monotonically as a function of G_N. This behavior can be better visualized in a three-dimensional plot (Fig. 1D) and a color-scale plot (Fig. 1E) that introduce an additional axis for G_N. The zero-bias conductance reaches a plateau when G_N is around 0.3 G_0 ($G_0 \equiv 2e^2/h$). Two plots of conductance curves as a function of G_N are extracted from Fig. 1, C to E. The zero-bias conductance barely changes over a wide range of G_N (0.3 G_0 ~ 0.9 G_0); the average plateau conductance (G_P) is equal to 0.64 G_0 (Fig. 1F). In contrast, the high-bias conductance at ±1.5 meV and -4.5 meV (Fig. 1G) changes by a factor of more than three as the tip-sample distance varies.

In order to examine the particle-hole-symmetric nature of the MZMs, we compare and contrast conductance behavior of zero-energy MZMs and finite-energy CBSs. As demonstrated previously, there are two distinct types of vortices, *i.e.* topological (ordinary) vortices with (without) MZM, differing by a half-integer level shift of vortex bound states (*18*). First, we perform a tunnel-coupling dependent measurement on a topological vortex (Fig. 2, A and B), which shows an MZM and the first CBS level located at 0 meV and ± 0.31 meV, respectively. In contrast to MZM, we find that the conductance of finite-energy CBS keeps increasing with G_N and shows no plateau. We also carry out measurements on an ordinary vortex. A *dI/dV* spectrum shows a CBS with half-odd-integer quantization (Fig. 2C), in which the first three levels of CBSs located at ±0.13 meV, ±0.39 meV and ±0.65 meV, respectively. Again, the conductance values of all the CBSs keep increasing and have no plateau feature in the tunnel-coupling dependent measurement (Fig. 2D). As another check, we repeat the measurement for the same location at zero magnetic field (Fig. 2, E and F), and observe a hard superconducting gap. The zero-bias conductance and the high-bias conductance are plotted as functions of G_N (middle and bottom panels of Fig. 2F, respectively). It is evident that both curves keep increasing as the tunnel coupling increases. This observation can be confirmed in a z-offset plot, with a larger z-offset corresponding to a smaller tip-sample distance (fig. S3). Therefore, the conductance plateau feature has only been observed in ZBCP, which indicates behavior unique to Majorana modes.

The plateau behavior of the zero-bias conductance provides evidence for the Majorana-induced resonant Andreev reflection (*19*, *20*). It has been well understood that a perfect transmission of electrons can occur in a symmetric double-barrier system via resonant tunneling through a single quasistationary bound state (Fig. 2G). The transmission on resonance is e^2/h independent of tunnel coupling, as long as it is identical for the two barriers (*28*, *29*). In the case of electron tunneling from a normal electrode through a barrier into a superconductor, the Andreev reflection process (*30*) converts the incident electron into an outgoing hole in the same electrode, resulting in a double-barrier system in the particle-hole Hilbert space. Moreover, in the case of Andreev reflection via a single MZM, the equal amplitude of particle/hole components, caused by the particle-antiparticle equivalence of MZM, ensures an identical tunnel coupling with electron and hole in the same electrode ($\Gamma_e = \Gamma_h$) (Fig. 2H). Thus, the resonant Andreev reflection mediated by an MZM leads to a $2e^2/h$-quantized zero-bias conductance plateau, independent of the strength of tunnel coupling at zero temperature (*19*, *20*, *31*, *32*). In contrast, low-energy CBSs (*33*, *34*) and other trivial sub-gap states (*22*) do not have the Majorana symmetry, resulting in unequal weights for electron/hole components. The relationship of $\Gamma_e = \Gamma_h$ is broken in a CBS-mediated Andreev reflection (Fig. 2I), which leads to an absence of a conductance plateau (middle panel in Fig. 2B). Moreover, the observed zero-bias conductance plateau in the vortex core disappears after the magnetic field is removed (Fig. 3, E and F), and hence cannot be attributed to quantum ballistic transport (*35*–*40*).

We observed the plateau behavior of ZBCPs repeatedly in many topological vortices [31 plateau features out of 60 measurements (*41*)]. We perform a statistical analysis of the observed plateau values G_p and find that most values of G_p are located around 40% to 60% of $G_0 = 2e^2/h$ (Fig. 3A). In one case, the plateau conductance reaches G_0 (Fig. 3, B to D). Both instrumental broadening and quasiparticle poisoning in our system can potentially induce deviation of G_p from the theoretical quantized value $2e^2/h$. To examine the possible effect of instrumental broadening on Majorana conductance plateau, we deliberately increase the instrumental broadening by varying the modulation voltage (V_{mod}), which is defined by the zero-to-peak amplitude of lock-in excitation. This allows us to study the V_{mod}-evolution of the Majorana conductance plateau on a given topological vortex (Fig. 3, E and F). We find that larger V_{mod} leads to stronger suppression of G_P of MZM. In addition, we notice that the values of conductance plateaus are correlated with the full width of half maximum (FWHM) of the ZBCP measured under a large tip-sample distance limit. We find that G_P decreases with increasing FWHM (Fig. 3G) (detailed data are shown in fig. S5). This indicates that the quasiparticle poisoning effect (*42*, *43*) might also play a role in reducing the conductance plateau value; the poisoning rate is expected to be spatially non-uniform in $FeTe_{0.55}Se_{0.45}$, which has intrinsic inhomogeneities.

We also checked the reversibility of the process of varying tunneling coupling in STM, and find that both the topography and the conductance plateau can be reproduced during two repeated sequences of varying tunneling coupling (fig. S8), indicating the absence of irreversible damage of the tip

and the sample during measurements. We note that other mechanisms related to zero-bias conductance plateau, such as inhomogeneity induced ps-ABS (*22*–*24*) and class-D weak antilocalization (*44*), cannot be definitively excluded; complete understanding of our experiments requires further theoretical efforts. Our observation of a zero-bias conductance plateau in the two-dimensional vortex case, which approaches the quantized conductance of $2e^2/h$, provides spatially-resolved spectroscopic evidence for Majorana-induced resonant electron transmission into a bulk superconductor, moving one step further toward the braiding operation applicable to topological quantum computation.

REFERENCES AND NOTES

1. A. Y. Kitaev, Fault-tolerant quantum computation by anyons. *Ann. Phys.* **303**, 2–30 (2003). doi:10.1016/S0003-4916(02)00018-0
2. C. Nayak, S. H. Simon, A. Stern, M. Freedman, S. Das Sarma, Non-Abelian anyons and topological quantum computation. *Rev. Mod. Phys.* **80**, 1083–1159 (2008). doi:10.1103/RevModPhys.80.1083
3. A. Y. Kitaev, Unpaired Majorana fermions in quantum wires. *Phys. Uspekhi* **44** (10S), 131–136 (2001). doi:10.1070/1063-7869/44/10S/S29
4. N. Read, D. Green, Paired states of fermions in two dimensions with breaking of parity and time-reversal symmetries and the fractional quantum Hall effect. *Phys. Rev. B Condens. Matter Mater. Phys.* **61**, 10267–10297 (2000). doi:10.1103/PhysRevB.61.10267
5. L. Fu, C. L. Kane, Superconducting proximity effect and majorana fermions at the surface of a topological insulator. *Phys. Rev. Lett.* **100**, 096407 (2008). doi:10.1103/PhysRevLett.100.096407 Medline
6. J. D. Sau, R. M. Lutchyn, S. Tewari, S. Das Sarma, Generic new platform for topological quantum computation using semiconductor heterostructures. *Phys. Rev. Lett.* **104**, 040502 (2010). doi:10.1103/PhysRevLett.104.040502 Medline
7. R. M. Lutchyn, J. D. Sau, S. Das Sarma, Majorana fermions and a topological phase transition in semiconductor-superconductor heterostructures. *Phys. Rev. Lett.* **105**, 077001 (2010). doi:10.1103/PhysRevLett.105.077001 Medline
8. Y. Oreg, G. Refael, F. von Oppen, Helical liquids and Majorana bound states in quantum wires. *Phys. Rev. Lett.* **105**, 177002 (2010). doi:10.1103/PhysRevLett.105.177002 Medline
9. V. Mourik, K. Zuo, S. M. Frolov, S. R. Plissard, E. P. A. M. Bakkers, L. P. Kouwenhoven, Signatures of Majorana fermions in hybrid superconductor-semiconductor nanowire devices. *Science* **336**, 1003–1007 (2012). doi:10.1126/science.1222360 Medline
10. R. M. Lutchyn, E. P. A. M. Bakkers, L. P. Kouwenhoven, P. Krogstrup, C. M. Marcus, Y. Oreg, Majorana zero modes in superconductor–semiconductor heterostructures. *Nat. Rev. Mater.* **3**, 52–68 (2018). doi:10.1038/s41578-018-0003-1
11. H. H. Sun, K.-W. Zhang, L.-H. Hu, C. Li, G.-Y. Wang, H.-Y. Ma, Z.-A. Xu, C.-L. Gao, D.-D. Guan, Y.-Y. Li, C. Liu, D. Qian, Y. Zhou, L. Fu, S.-C. Li, F.-C. Zhang, J.-F. Jia, Majorana Zero Mode Detected with Spin Selective Andreev Reflection in the Vortex of a Topological Superconductor. *Phys. Rev. Lett.* **116**, 257003 (2016). doi:10.1103/PhysRevLett.116.257003 Medline
12. S. Nadj-Perge, I. K. Drozdov, B. A. Bernevig, A. Yazdani, Proposal for realizing Majorana fermions in chains of magnetic atoms on a superconductor. *Phys. Rev. B Condens. Matter Mater. Phys.* **88**, 020407 (2013). doi:10.1103/PhysRevB.88.020407
13. S. Nadj-Perge, I. K. Drozdov, J. Li, H. Chen, S. Jeon, J. Seo, A. H. MacDonald, B. A. Bernevig, A. Yazdani, Topological matter. Observation of Majorana fermions in ferromagnetic atomic chains on a superconductor. *Science* **346**, 602–607 (2014). doi:10.1126/science.1259327 Medline
14. Z. Wang, P. Zhang, G. Xu, L. K. Zeng, H. Miao, X. Xu, T. Qian, H. Weng, P. Richard, A. V. Fedorov, H. Ding, X. Dai, Z. Fang, Topological nature of the FeSe 0.5 Te 0.5 superconductor. *Phys. Rev. B Condens. Matter Mater. Phys.* **92**, 115119 (2015). doi:10.1103/PhysRevB.92.115119
15. P. Zhang, K. Yaji, T. Hashimoto, Y. Ota, T. Kondo, K. Okazaki, Z. Wang, J. Wen, G. D. Gu, H. Ding, S. Shin, Observation of topological superconductivity on the surface of an iron-based superconductor. *Science* **360**, 182–186 (2018). doi:10.1126/science.aan4596 Medline
16. D. Wang, L. Kong, P. Fan, H. Chen, S. Zhu, W. Liu, L. Cao, Y. Sun, S. Du, J. Schneeloch, R. Zhong, G. Gu, L. Fu, H. Ding, H.-J. Gao, Evidence for Majorana bound states in an iron-based superconductor. *Science* **362**, 333–335 (2018). doi:10.1126/science.aao1797 Medline
17. T. Machida, Y. Sun, S. Pyon, S. Takeda, Y. Kohsaka, T. Hanaguri, T. Sasagawa, T. Tamegai, Zero-energy vortex bound state in the superconducting topological surface state of Fe(Se,Te). *Nat. Mater.* **18**, 811–815 (2019). doi:10.1038/s41563-019-0397-1 Medline
18. L. Kong *et al.*, *Nat. Phys.* (2019). 10.1038/s41567-019-0630-5
19. K. T. Law, P. A. Lee, T. K. Ng, Majorana fermion induced resonant Andreev reflection. *Phys. Rev. Lett.* **103**, 237001 (2009). doi:10.1103/PhysRevLett.103.237001 Medline
20. M. Wimmer, A. R. Akhmerov, J. P. Dahlhaus, C. W. J. Beenakker, Quantum point contact as a probe of a topological superconductor. *New J. Phys.* **13**, 053016 (2011). doi:10.1088/1367-2630/13/5/053016
21. H. Zhang, C.-X. Liu, S. Gazibegovic, D. Xu, J. A. Logan, G. Wang, N. van Loo, J. D. S. Bommer, M. W. A. de Moor, D. Car, R. L. M. Op Het Veld, P. J. van Veldhoven, S. Koelling, M. A. Verheijen, M. Pendharkar, D. J. Pennachio, B. Shojaei, J. S. Lee, C. J. Palmstrøm, E. P. A. M. Bakkers, S. D. Sarma, L. P. Kouwenhoven, Quantized Majorana conductance. *Nature* **556**, 74–79 (2018). doi:10.1038/nature26142 Medline
22. C. X. Liu, J. D. Sau, T. D. Stanescu, S. Das Sarma, Andreev bound states versus Majorana bound states in quantum dot-nanowire-superconductor hybrid structures: Trivial versus topological zero-bias conductance peaks. *Phys. Rev. B* **96**, 075161 (2017). doi:10.1103/PhysRevB.96.075161
23. C. Moore, T. D. Stanescu, S. Tewari, Two-terminal charge tunneling: Disentangling Majorana zero modes from partially separated Andreev bound states in semiconductor-superconductor heterostructures. *Phys. Rev. B* **97**, 165302 (2018). doi:10.1103/PhysRevB.97.165302
24. C. Moore, C. C. Zeng, T. D. Stanescu, S. Tewari, Quantized zero-bias conductance plateau in semiconductor-superconductor heterostructures without topological Majorana zero modes. *Phys. Rev. B* **98**, 155314 (2018). doi:10.1103/PhysRevB.98.155314
25. Q. Liu, C. Chen, T. Zhang, R. Peng, Y.-J. Yan, C.-H.-P. Wen, X. Lou, Y.-L. Huang, J.-P. Tian, X.-L. Dong, G.-W. Wang, W.-C. Bao, Q.-H. Wang, Z.-P. Yin, Z.-X. Zhao, D.-L. Feng, Robust and Clean Majorana Zero Mode in the Vortex Core of High-Temperature Superconductor (Li 0.84 Fe 0.16) OHFeSe. *Phys. Rev. X* **8**, 041056 (2018). doi:10.1103/PhysRevX.8.041056
26. C. Chen, Q. Liu, T. Z. Zhang, D. Li, P. P. Shen, X. L. Dong, Z.-X. Zhao, T. Zhang, D. L. Feng, Quantized Conductance of Majorana Zero Mode in the Vortex of the Topological Superconductor ($Li_{0.84}Fe_{0.16}$)OHFeSe. *Chin. Phys. Lett.* **36**, 057403 (2019). doi:10.1088/0256-307X/36/5/057403
27. Materials and methods are available as supplementary materials.
28. R. Tsu, L. Esaki, Tunneling in a finite superlattice. *Appl. Phys. Lett.* **22**, 562–564 (1973). doi:10.1063/1.1654509
29. L. L. Chang, L. Esaki, R. Tsu, Resonant tunneling in semiconductor double barriers. *Appl. Phys. Lett.* **24**, 593–595 (1974). doi:10.1063/1.1655067
30. G. E. Blonder, M. Tinkham, T. M. Klapwijk, Transition from metallic to tunneling regimes in superconducting microconstrictions: Excess current, charge imbalance, and supercurrent conversion. *Phys. Rev. B Condens. Matter* **25**, 4515–4532 (1982). doi:10.1103/PhysRevB.25.4515
31. K. Flensberg, Tunneling characteristics of a chain of Majorana bound states. *Phys. Rev. B Condens. Matter Mater. Phys.* **82**, 180516 (2010). doi:10.1103/PhysRevB.82.180516
32. F. Setiawan, C. X. Liu, J. D. Sau, S. Das Sarma, Electron temperature and tunnel coupling dependence of zero-bias and almost-zero-bias conductance peaks in Majorana nanowires. *Phys. Rev. B* **96**, 184520 (2017). doi:10.1103/PhysRevB.96.184520
33. C. Caroli, P. G. De Gennes, J. Matricon, Bound Fermion states on a vortex line in a type II superconductor. *Phys. Lett.* **9**, 307–309 (1964). doi:10.1016/0031-9163(64)90375-0

34. H. F. Hess, R. B. Robinson, J. V. Waszczak, Vortex-core structure observed with a scanning tunneling microscope. *Phys. Rev. Lett.* **64**, 2711–2714 (1990). doi:10.1103/PhysRevLett.64.2711 Medline
35. C. W. Beenakker, J. G. Williamson, L. P. Kouwenhoven, C. T. Foxon, Quantized conductance of point contacts in a two-dimensional electron gas. *Phys. Rev. Lett.* **60**, 848–850 (1988). doi:10.1103/PhysRevLett.60.848 Medline
36. J. Kammhuber, M. C. Cassidy, H. Zhang, Ö. Gül, F. Pei, M. W. A. de Moor, B. Nijholt, K. Watanabe, T. Taniguchi, D. Car, S. R. Plissard, E. P. A. M. Bakkers, L. P. Kouwenhoven, Conductance Quantization at Zero Magnetic Field in InSb Nanowires. *Nano Lett.* **16**, 3482–3486 (2016). doi:10.1021/acs.nanolett.6b00051 Medline
37. C. W. Beenakker, Quantum transport in semiconductor-superconductor microjunctions. *Phys. Rev. B Condens. Matter* **46**, 12841–12844 (1992). doi:10.1103/PhysRevB.46.12841 Medline
38. M. Kjaergaard, F. Nichele, H. J. Suominen, M. P. Nowak, M. Wimmer, A. R. Akhmerov, J. A. Folk, K. Flensberg, J. Shabani, C. J. Palmstrøm, C. M. Marcus, Quantized conductance doubling and hard gap in a two-dimensional semiconductor-superconductor heterostructure. *Nat. Commun.* **7**, 12841 (2016). doi:10.1038/ncomms12841 Medline
39. H. Zhang, Ö. Gül, S. Conesa-Boj, M. P. Nowak, M. Wimmer, K. Zuo, V. Mourik, F. K. de Vries, J. van Veen, M. W. A. de Moor, J. D. S. Bommer, D. J. van Woerkom, D. Car, S. R. Plissard, E. P. A. M. Bakkers, M. Quintero-Pérez, M. C. Cassidy, S. Koelling, S. Goswami, K. Watanabe, T. Taniguchi, L. P. Kouwenhoven, Ballistic superconductivity in semiconductor nanowires. *Nat. Commun.* **8**, 16025 (2017). doi:10.1038/ncomms16025 Medline
40. Ö. Gül, H. Zhang, J. D. S. Bommer, M. W. A. de Moor, D. Car, S. R. Plissard, E. P. A. M. Bakkers, A. Geresdi, K. Watanabe, T. Taniguchi, L. P. Kouwenhoven, Ballistic Majorana nanowire devices. *Nat. Nanotechnol.* **13**, 192–197 (2018). doi:10.1038/s41565-017-0032-8 Medline
41. That we did not observe a plateau feature in the other 29 cases is because of the instability of the vortices during the tip-approaching process [(*27*), section 5].
42. J. R. Colbert, P. A. Lee, Proposal to measure the quasiparticle poisoning time of Majorana bound states. *Phys. Rev. B Condens. Matter Mater. Phys.* **89**, 140505 (2014). doi:10.1103/PhysRevB.89.140505
43. I. Martin, D. Mozyrsky, Nonequilibrium theory of tunneling into a localized state in a superconductor. *Phys. Rev. B Condens. Matter Mater. Phys.* **90**, 100508 (2014). doi:10.1103/PhysRevB.90.100508
44. W. S. C. Haining Pan, D. Jay, Sau and S. Das Sarma, *arXiv:1906.08193*, (2019).
45. S. Zhu *et al.*, Nearly quantized conductance plateau of vortex zero mode in an iron-based superconductor. Zenodo (2019); doi:10.5281/zenodo.3514211
46. J. Wen, G. Xu, Z. Xu, Z. W. Lin, Q. Li, W. Ratcliff, G. Gu, J. M. Tranquada, Short-range incommensurate magnetic order near the superconducting phase boundary in Fe 1 + δ Te 1 − x Se x. *Phys. Rev. B Condens. Matter Mater. Phys.* **80**, 104506 (2009). doi:10.1103/PhysRevB.80.104506
47. T. Machida, Y. Kohsaka, T. Hanaguri, A scanning tunneling microscope for spectroscopic imaging below 90 mK in magnetic fields up to 17.5 T. *Rev. Sci. Instrum.* **89**, 093707 (2018). doi:10.1063/1.5049619 Medline
48. R. C. Dynes, V. Narayanamurti, J. P. Garno, Direct Measurement of Quasiparticle-Lifetime Broadening in a Strong-Coupled Superconductor. *Phys. Rev. Lett.* **41**, 1509–1512 (1978). doi:10.1103/PhysRevLett.41.1509

ACKNOWLEDGMENTS

We thank Patrick A. Lee, Chun-Xiao Liu, Gang Su for helpful discussions, and Ai-Wei Wang, Jia-Hao Yan and Qing Huan for technical assistance. **Funding:** The work at IOP is supported by grants from the Ministry of Science and Technology of China (2015CB921000, 2015CB921300, 2016YFA0202300), the National Natural Science Foundation of China (11234014, 61888102), and the Chinese Academy of Sciences (XDB28000000, XDB07000000, 112111KYSB20160061). L.F. and G.G are supported by US DOE (DE-SC0010526, DE-SC0012704, respectively). J.S. and R.Z. are supported by the Center for Emergent Superconductivity, an EFRC funded by the US DOE. **Author Contributions:** H.-J. G. and H.D. designed STM experiments. S.Z., L.C., H.C., Y.X. and Y.Z. performed STM experiments with assistance of W.L., F.Y. and C. S. J.S., R.Z., and G.G. provided samples. L.F. provided theoretical explanations. Y.Z., S.D., S.Z. and L.K. processed experimental data and wrote the manuscript. All the authors participated in analyzing experimental data, plotting figures, and writing the manuscript. H.D. and H.-J. G. supervised the project. **Competing interests:** The authors declare that they have no competing interests. **Data and materials availability:** The data presented in this paper can be found in (*45*).

SUPPLEMENTARY MATERIALS

science.sciencemag.org/cgi/content/full/science.aaz0274/DC1
Materials and Methods
Supplementary Text
Figs. S1 to S9
References (*46–48*)

15 February 2019; resubmitted 29 July 2019
Accepted 7 November 2019
Published online 12 December 2019
10.1126/science.aax0274

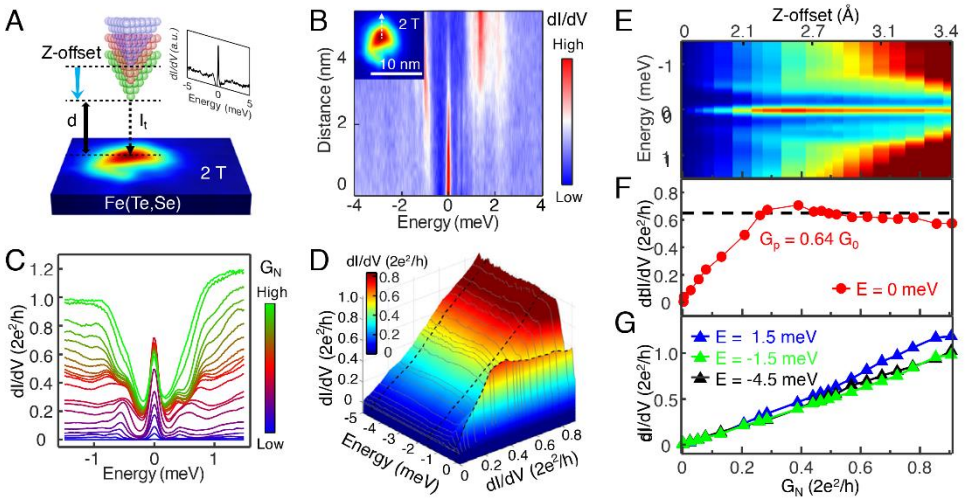

Fig. 1. Zero-bias conductance plateau observed on $FeTe_{0.55}Se_{0.45}$. (**A**) A schematic of variable tunnel coupling STM/S method. A zero-bias conductance map under 2.0 T is shown on a sample surface. A *dI/dV* spectrum measured at the center of the vortex core (V_s = −5 mV, I_t = 500 pA, V_{mod} = 0.02 mV) is shown in the right-top inset; a sharp zero-bias conductance peak (ZBCP) is observed. When the tunneling current (I_t) is adjusted by the STM regulation loop, the tunnel coupling between the STM tip and the MZM can be tuned continuously by the tip-sample distance (*d*). Larger tunnel coupling corresponds to smaller *d* and larger tunneling-barrier conductance ($G_N = I_t/V_s$, V_s is the setpoint voltage). *z*-offset can be read out simultaneously, which indicates the absolute z-direction motion of the STM tip. (**B**) A line-cut intensity plot along the dashed white arrow in the inset, measured from the same vortex shown in (A), showing a stable MZM across the vortex core. (**C**) An overlapping plot of *dI/dV* spectra under different tunnel coupling values parameterized in G_N. The blue curve is measured under the smallest G_N whereas the green curve with the largest G_N. (**D**) A three-dimensional plot of tunnel coupling dependent measurement, $dI/dV(E, G_N)$. For clarity, only the data points in the energy range of [-5.0, 0.2] meV are shown. (**E**) A color-scale plot of (C) within the energy range of [-1.5, 1.5] meV that shows the spectra as a function of G_N. The *z*-offset information, which was taken simultaneously by STM, is provided on the upper axis. The maximum distance the tip approached is 3.4 Å. This plot shares the same color-bar with (D). (**F**) A horizontal line-cut at the zero-bias from (E). The conductance curve shows a plateau behavior with the plateau conductance (G_P) equal to (0.64 ± 0.04) G_0. (**G**) Horizontal line-cuts at high-bias values from (E). The absence of a conductance plateau on these curves indicates conventional tunneling behavior at the energy of continuous states. All the data are measured at T_{eff} = 377 mK.

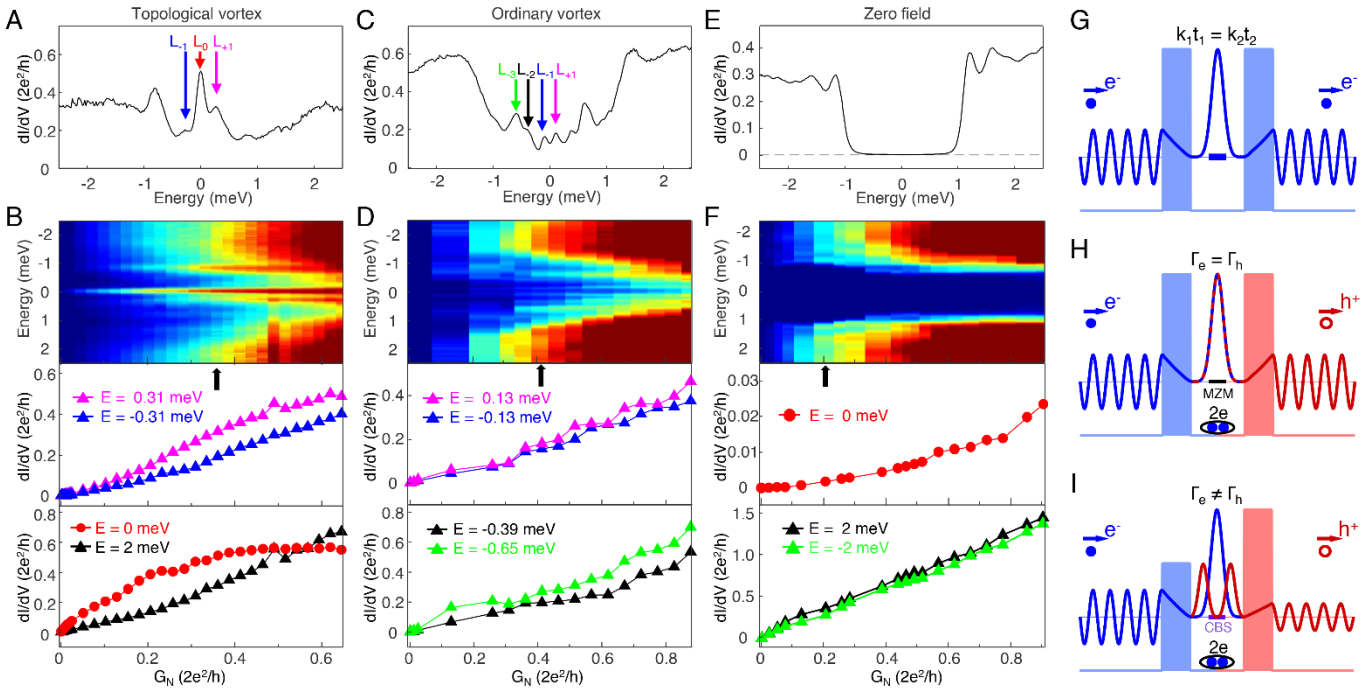

Fig. 2. Majorana induced resonant Andreev reflection. (**A**) A *dI/dV* spectrum measured at the center of a topological vortex (V_s = –5 mV, I_t = 140 nA, V_{mod} = 0.02 mV), which shows an MZM (red arrow) coexisting with CBSs located at ±0.31 meV (marked by magenta and blue arrows). (**B**) A tunnel coupling dependent measurement on the vortex shown in (A) at 2 T. Top panel: a color-scale plot, $dI/dV(E, G_N)$. The G_N position of (A) is marked by a black arrow. Middle panel: tunnel coupling evolution of CBS conductance, which shows no plateau behavior. Bottom panel: tunnel coupling evolution of conductance at the energies of 0 meV (red circles, exhibiting a plateau) and 2 meV (black triangles, monotonically increasing). (**C**) A *dI/dV* spectrum measured at the center of an ordinary vortex (V_s = -5 mV, I_t = 160 nA, V_{mod} = 0.02 mV), which clearly shows three levels of CBS at ±0.13 meV (magenta and blue arrows), ±0.39 meV (black arrow) and ±0.65 meV (green arrow). (**D**) Similar to (B), but measured on the vortex shown in (C). Middle and bottom panels: tunnel coupling evolution of CBS conductance, showing no plateau feature. (**E**) A *dI/dV* spectrum measured at 0 T (V_s = –5 mV, I_t = 80 nA, V_{mod} = 0.02 mV). A hard superconducting gap can be seen. (**F**) Similar to (B) and (D), but measured under 0 T. Middle panel: tunnel coupling evolution of zero-bias conductance (normal metal - superconductor junction case). Bottom panel: tunnel coupling evolution of conductance at the above gap energy (normal metal - normal metal junction case). There is no plateau behavior at 0 T. (**G**) A schematic of resonant tunneling through a symmetric double barrier system. The wavefunction evolution of a tunneled electron is shown. *kt* is penetration constant. (**H**) The double-barrier view of the MZM-induced resonant Andreev reflection. The blue and red colors indicate the electron and hole process, respectively. The equivalence of particle and hole components in MZM ensures the same tunnel coupling on electron and hole barrier ($\Gamma_e = \Gamma_h$). (**I**) The double-barrier view of Andreev reflection mediated by a CBS. The arbitrary mixing of particle-hole components in CBS breaks the resonance condition. All the data are measured at T_{eff} = 377 mK.

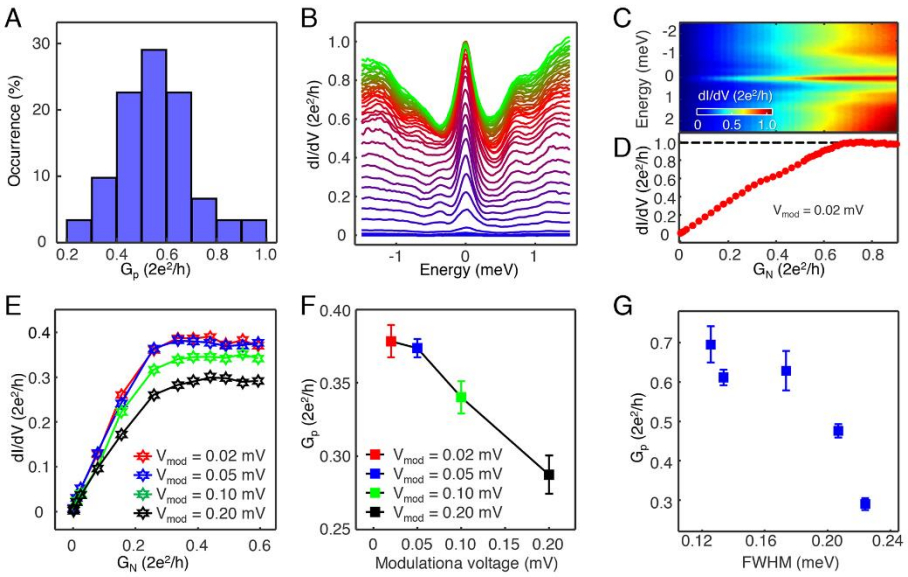

Fig. 3. The conductance variation of Majorana plateau. (**A**) A histogram of the G_p from 31 sets of data which are measured with the same instrument. Sorting of the plateau conductance (G_p) in the order of increasing magnitude can be found in fig. S9. (V_s = −5 mV, V_{mod} = 0.02 mV) (**B**) The overlapping plot of 38 *dI/dV* spectra selected from a topological vortex that reaches a quantized conductance plateau. (V_s = −5 mV, V_{mod} = 0.02 mV) (**C**) A color-scale plot of (B) within the energy range of [−2.5, 2.5] meV that shows the spectra as a function of G_N. (**D**) A horizontal line-cut at the zero-bias from (C). The conductance curve shows the conductance plateau reaches G_0. (**E**) A series of tunnel coupling dependent measurements on the same MZM, with four modulation voltages of 0.02 mV, 0.05 mV, 0.10 mV and 0.20 mV. (**F**) The plot of G_P as a function of modulation voltage of the data shown in (E). (**G**) Relationship between FWHM of ZBCP and G_P, obtained from five different MZMs measured at the same experimental conditions, suggesting that the quasiparticle poisoning effect affects the plateau value. The FWHM were extracted from the spectrum measured at a large tip-sample distance with the same experimental parameters (V_s = −5 mV, I_t = 500 pA, V_{mod} = 0.02 mV). All the data are measured at T_{eff} = 377 mK.

Nearly quantized conductance plateau of vortex zero mode in an iron-based superconductor

Shiyu Zhu, Lingyuan Kong, Lu Cao, Hui Chen, Michal Papaj, Shixuan Du, Yuqing Xing, Wenyao Liu, Dongfei Wang, Chengmin Shen, Fazhi Yang, John Schneeloch, Ruidan Zhong, Genda Gu, Liang Fu, Yu-Yang Zhang, Hong Ding and Hong-Jun Gao

published online December 12, 2019